Energy efficient design of regenerative shock absorbers for automotive suspensions: A multi-objective optimization framework

Preprint version

Full paper available at https://www.sciencedirect.com/science/article/pii/S0306261923019062
DOI: https://doi.org/10.1016/j.apenergy.2023.122542

Energy Efficient Design of Regenerative Shock Absorbers for Automotive Suspensions: A Multi-Objective Optimization Framework

Marco Puliti[a,b], Renato Galluzzi[c], Federico Tessari[d], Nicola Amati[a], Andrea Tonoli[a]

[a]*Mechatronics Laboratory (LIM), Politecnico di Torino, Italy*
[b]*Rehab Technologies INAIL-IIT Lab, Italian Institute of Technology, Italy*
[c]*School of Engineering and Sciences, Tecnologico de Monterrey, Mexico*
[d]*Laboratory for Biomechanics and Human Rehabilitation, Massachusetts Institute of Technology, United States*

Abstract

Over the last decade, the automotive industry has faced several challenges to reduce vehicle's emissions, moving towards more efficient wheeled transportation. Among all, automotive suspension systems are becoming key players in reducing the carbon footprint of vehicles. In this context, regenerative shock absorbers (RSAs) have been employed to recover vibrational energy from the interaction between road irregularities and vehicle, throughout the suspension unit. Recently, electro-hydrostatic regenerative shock absorbers (EHRSAs) gained scientific interest due to their advantages in terms of power to weight ratio and compactness, when compared with other regenerative systems. However, their design requires a trade-off among opposite objectives, such as performance and size. In practice, such compromise is often left to the designer expertise. To address such issue, this work proposes a design optimization strategy for gerotor-based EHRSAs, with the aim of maximizing regeneration efficiency and harvestable energy while minimizing size and weight. The optimization problem is dealt considering a multi-objective, evolutionary genetic algorithm (GA), exploited to find an optimal EHRSA design. First, a numerical analysis was conducted to preliminary validate the optimization framework. Then, such methodology is applied to design an EHRSA prototype and experiments are conducted to evaluate its performance. Finally, a quarter car model of a class J vehicle and a linear quadratic regulator (LQR) control strategy are exploited to compare the EHRSA power regeneration performance with respect to state of the art regenerative shock absorbers. Results show an average regenerated power of 101 W per shock absorber, corresponding to 5.25 g/km of CO_2 emission reduction estimate according to the European technical guidelines for eco-innovation.

Keywords: Efficiency-driven design, Energy harvesting, Energy management, Regenerative shock absorber, Electro-hydrostatic actuation, Multi-objective optimization

1. Introduction

In the last decade, the automotive industry has faced more strict regulations in terms of carbon dioxide (CO_2) emissions to address the environmental concerns worldwide. In 2017, road transportation accounted for 21% of the European Union's total CO_2 emissions. In 2020, the average CO_2 vehicle's emissions was bound to 95 g/km. Such value is planned to be further reduced by 15% in 2025 and by 37.5% in 2030 [1]. The arising need to reduce the carbon footprint of wheeled vehicles has led the automotive industry to explore innovative solutions to improve the overall energy efficiency of wheeled transportation. Although the main target is the vehicle engine, the suspension system can play a crucial role. Its main task is to filter out vibrations associated to the vehicle interactions with the road profile. At a system level, such behaviour reflects in an improvement of vehicle handling and comfort. Traditional suspension systems are passive, meaning that the vibrational energy is completely dissipated. On the other hand, semi-active and active suspension systems can successfully recover part of such vibrational energy and convert it into electrical one [2].

From an energetic viewpoint, it has been demonstrated that such regenerative energy can be directly related to vehicle's CO_2 emission reductions. Namely, such energy is proportional to tyre stiffness, vehicle speed and road roughness index defined by the International Standard Organization (ISO) [3]. Considering an ISO C-class road profile, the maximum power that can be dissipated is around 130W [4]. Then, the CO_2 reduction for a D-class vehicle in such conditions would be around 6 g/km [5], representing 6.3 % of the 2020 CO_2 emission bound. These figures motivate the development of novel suspension systems, with the aim of maximizing the conversion efficiency and reduce the carbon footprint of wheeled vehicles.

In general, suspension systems feature an elastic element in parallel with a damping device, often called shock absorber. Depending on the shock absorber technology, they can be differentiated into passive, semi-active and active devices [2]. The conventional type is passive, in which the aim is to dissipate vibrational energy into heat. Despite simple and cost-effective design, passive solutions are not able to adapt to changes both at vehicle and road level, providing a fixed damping response. On the other hand, semi-active solutions can provide a discrete damping behavior, exploiting finite states of passive damping response.

More recently, the research focus has been directed towards active suspension systems. The damping element is replaced by an actuation unit, capable of adapting its damping behaviour on demand. The actuation device can be referred as regenerative shock absorber (RSA) if the vibrational energy can be partly converted into electrical one. Namely, an RSA features an electric machine and a suitable transmission system. The harvesting capabilities are provided by the intrinsic reversibility of the electric machine, working as motor when actuating and as generator when recovering energy. Regenerative shock absorbers can either feature a linear or a rotary electric machine. It would seem straightforward to exploit linear motors since their integration in the suspension layout would be simple and there may be no need for a transmission system. However, their power to weight ratio is limited when compared to rotary solutions of the same size [6]. Hence, rotary electric machines are often the preferable option, although a transmission system to convert linear motion into angular displacement is needed. Currently, the automotive industry mainly relies on mechanical and hydraulic transmission systems. The mechanical most common solutions are ball screw mechanisms[7], gearboxes [8] or rack pinion transmissions [9]. Although they are efficient devices, wear and fatigue are critical aspects for high duty-cycle tasks such as in vehicles suspension systems.

On the other hand, hydraulic solutions mainly comprehend a hydraulic cylinder coupled with flow control valves or hydraulic pumps. Among all, electro-hydrostatic actuators (EHAs) have gained particular interest in applications such as regenerative shock absorbers. They are closed-circuit transmission systems, featuring an electric motor that drives a bidirectional hydraulic machine, used to regulate the pressure difference and fluid flow inside a hydraulic actuator, as schematized in Figure 1. EHAs combine key benefits of hydraulic and mechanical actuation. As their conventional hydraulic counterpart, EHAs deliver a high power-to-mass ratio. In addition, they preserve a quasi-rigid coupling between the actuation chain and the load, thus attaining large bandwidth dynamics and accurate motion control [10]. In applications where maintainability and reliability are relevant driving factors, EHA represents a solid alternative to electro-mechanical technologies, as weight and size are significantly lower [11]. The concept behind EHA systems is hydrostatic transmission or continuous variable transmission, in which the medium for converting motion between rotary and linear domains is the fluid. Hence, advantageous placement within the suspension layout can be achieved. Recent works addressed such technology in the context of damping devices. Galluzzi et al. proposed an EHA prototype for helicopter rotor blade lead-lag damping [12], Zhang et al. investigated an hydraulic regenerative shock absorber solution for off-road vehicles [13]. Other EHA applications are related to the robotics field [14–17] and aerospace actuation systems [18].

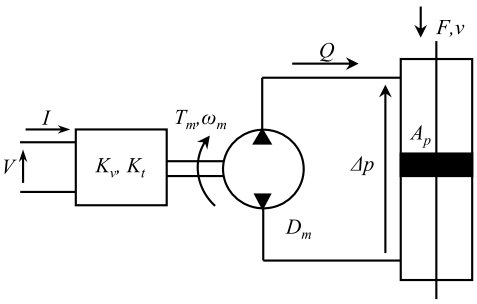

Figure 1: EHA system schematic in actuation mode

In the context of suspension systems, EHAs can be addressed as electro-hydrostatic regenerative shock absorbers (EHRSAs). Their design directly affects the harvesting capabilities of the suspension system and it often represents a trade-off among opposite objectives, such as performance and size. Previous research dealt with the design of single sub-systems [19, 20], or by using off-the-shelf components. Optimizing such system is non-trivial, as different physical domains are coupled together and the design is application oriented. Since, each application requires different design targets, EHAs design represents a multi-objective optimization (MOO) problem.

Although the state of the art has addressed the design of EHRSAs, an optimized design methodology for energy harvesting purposes is still missing. In the attempt to close such gap, the present paper proposes a novel design framework for EHRSA systems based on evolutionary genetic algorithms. By solving an MOO problem, the aim is to maximize the conversion efficiency and harvesting capabilities whilst yielding a compact and performant active shock absorber. Numerical models are used to preliminary validate the optimization strategy. Then, an EHRSA prototype is developed and an experimental campaign is performed to assess the device shock absorbing capabilities. Finally, experimental results are exploited to develop a quarter car model. The EHRSA is modeled considering the experimental efficiency maps and the harvestable energy is maximized considering an energy-oriented control strategy. Results are presented in terms of regeneration efficiency, average power regenerated and estimate of CO_2 reduction.

2. Multi-Objective Optimization Methodology

The workflow of the presented optimization framework is schematized in Fig. 2. The modeling phase defines the analytical models of each EHA sub-component. Then, the MOO phase concerns stating the design variables, constraints, and objective functions for the optimization algorithm. As for the modeling phase, linear or rotary EHA topology can be chosen. The authors decided to focus on a linear application due to its wider adoption. Additionally, the intrinsic reversibility of the electric machine can be exploited for two different tasks, actuation and regeneration. It is worth to mention that just a fraction of the hydraulic energy can be effectively converted by the electric machine since each component carries inevitable energy losses.

2.1. Hydraulic cylinder

A through rod cylinder is considered to account for actuator compactness. It allows to avoid the use of a hydraulic accumulator to compensate for flow rate drops among cylinder's

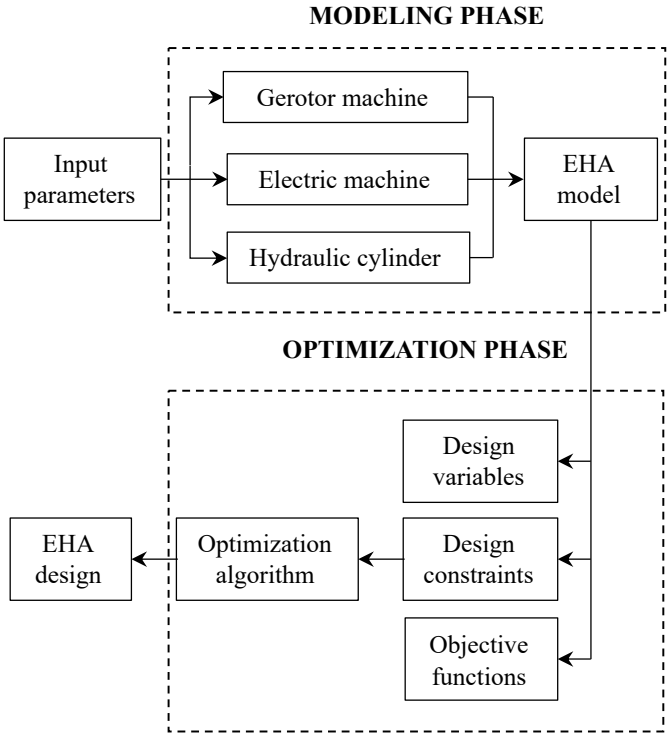

Figure 2: Workflow of the EHA design optimization framework

chambers. Generally, it can be defined with two parameters: piston area A_p and piston stroke s. The former is related to the force exerted by the actuator and its load, whereas the latter accounts for the maximum travel of the actuator, thus defining its operating range. Independently from the application, the minimum requirements to size such component are two operating points in the Force-speed plane. Lastly, a hydraulic cylinder is characterized by both mechanical and hydraulic losses due to mechanical friction and hydraulic leakages. These are taken into account by means of an overall efficiency η_c, that in first approximation can be considered as constant.

2.2. Gerotor machine

Gerotor machines are hydraulic, internal gear units, characterized by an inner and outer rotor, rotating eccentrically. They are employed in several low-pressure applications (i.e., up to 100 bar [21]), for their greater compactness and resistance to wear and noise if compared to external gear machines. The outer gear features N teeth, one more than the inner one, resorting in a relative angular speed among them [22]. Gerotors are positive displacement components, in which the flow rate is generated by the periodical suction and delivery actions of the N chambers generated during gears meshing [23]. From a geometrical point of view, Tessari et al. provided an extensive design methodology to optimize the 2D section of gerotors, aiming to improve the component performance while minimizing leakages [19, 24]. These works are used as benchmark to analytically model the component.

First, the maximum flow rate Q_{max} and pressure differential Δp_{max} on the gerotor side are computed starting from the system requirements and the hydraulic cylinder characteristics. Namely,

$$Q_{max} = \frac{A_p\ v_{max}}{\eta_c}, \quad \Delta p_{max} = \frac{F_{max}}{A_p\ \eta_c} \tag{1}$$

in which v_{max} and F_{max} represent the cylinder speed and force requirements, respectively; whereas, η_c is the hydraulic cylinder efficiency. Then, the theoretical, gerotor maximum torque T_{max} and power P_{max} can be computed as follows

$$\begin{aligned} T_{max} &= D_m(D_g, L_g)\ \Delta p_{max}, \\ P_{gmax} &= T_{max}\ \omega_g = \frac{P_{max}}{\eta_c} \end{aligned} \tag{2}$$

where ω_g is the inner gear angular speed and D_m is the machine volumetric displacement, function of its external diameter D_g and axial length L_g. The second row of Eq.2 represents the gerotor power in nominal conditions, neglecting losses. To account for them, Harrison et al. proposed a 1D orifice model to analytically quantify viscous and friction losses in gerotor devices [25]. Within the presented work, losses due to axial and radial clearances between gerotor and its housing have been considered. Integrating Eq. 2 with the power loss contributions, the gerotor overall efficiency η_g can be quantified as

$$\eta_g = \frac{P_{g\ max}}{P_{g\ max} + P_{f1} + P_{f2}} = f(D_g, L_g) \tag{3}$$

where P_{f1} and P_{f2} represent axial and radial power losses, respectively.

2.3. Brushless DC electric machine

Brushless DC electric machine are commonly used in EHA systems. Specifically, the presented optimization methodology exploits a permanent magnet synchronous machine (PMSM). Since magnetic, electric and mechanical domains are coupled, it is quite complex to analytically model such machines. Hanselman provided a set of guidelines to model PMSM in an analytical fashion [26]. However, when the machine 2D section becomes too complex, finite element based models are the preferred design paradigm to better estimate the component's performance. In the context of this research, the electrical machine has been first modeled according to the characteristic equations provided in [26] and then refined performing a parametric finite element analysis (FEA). The chosen topology is a radial flux electric machine with slotted stator and surface-mounted permanent magnets. The main constraints from magnetic and electric domains are expressed in Table 1, considering [26]. The FEA outcome is the peak torque per unit meter T_{pm}

$$T_{pm} = \frac{k_t I_{ph}}{L_m} \tag{4}$$

Table 1: Permanent Magnet electric machine main parameters

Symbol	Value	Description
N_{ph}	3	Number of phases
B_r	1.4	Magnetic remanence [T]
B_{max}	1.5	Maximum magnetic flux density [T]
J_p	20	Peak current density [A/mm^2]
J_c	6	Continuous current density [A/mm^2]

in which I_{ph} is the phase current and L_m is the machine axial length, normalized to 1 meter. Overall, combining Eq.4, the parameters of Table 1 and the geometrical and electrical relationships provided in [26], it is possible to model the 2D section of the PMSM.

Fig. 3 presents the torque per meter FEA results and extrapolated fitting function for a suitable set of PMSM diameters D_s. A quadratic fitting function tracks appropriately the numerical results. Therefore, it can be used to model the PMSM torque per meter T_{pm} within the optimization algorithm, significantly reducing the algorithm computational time. Finally, the electric machine efficiency η_m should be included and can be considered constant in first approximation since the MOO considers the EHA nominal operating condition.

2.4. MOO problem formulation

An MOO problem is formulated considering the proposed design model and variables, objective functions and constraint conditions [27]. Mathematically, it can be written as:

$$\begin{aligned} &\min \{f_1(\mathbf{X}), f_2(\mathbf{X}),\ \dots, f_m(\mathbf{X})\} \\ &\text{s.t. } \{g_i(\mathbf{X}) \le 0,\ i = 0, 1,\ \dots, p\}, \\ &\quad \{h_j(\mathbf{X}) = 0,\ j = 0, 1,\ \dots, q\} \\ &\quad \mathbf{X}_L \le \mathbf{X} \le \mathbf{X}_U,\ \mathbf{X} = [x_1, x_2,\ \dots, x_n]^\intercal \end{aligned} \tag{5}$$

being $f_m(\mathbf{X})$ the m_{th} objective function, $g_i(\mathbf{X})$ the i_{th} inequality constraint, $h_j(\mathbf{X})$ the j_{th} equality constraint and $\mathbf{X}$ the vector of

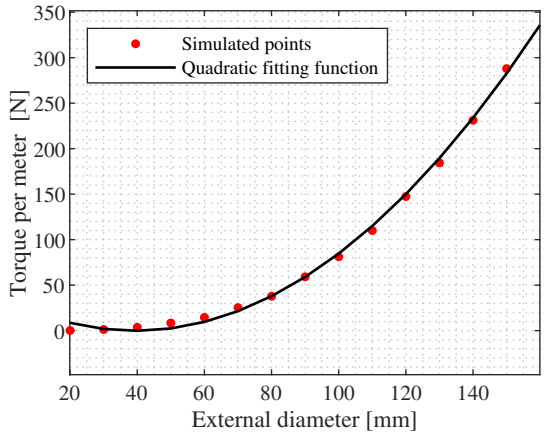

Figure 3: Numerical characterization of the torque per meter T_{pm} as function of the machine external diameter D_s

design variables. Additionally, $\mathbf{X}_L$ and $\mathbf{X}_U$ represent the vectors of lower and upper bounds, respectively. Such constraints define the variables space, $\mathbf{R}^n$, in which the algorithm can span to search for optimal solutions.

The choice of the design variables is non-trivial as they should be independent and minimized without constraining the design possibilities. The presented optimization framework exploits the PMSM diameter D_s, its length L_m and the gerotor machine axial length L_g as design variables. Other relevant parameters are the gerotor diameter D_g and the hydraulic cylinder diameter D_p, not included but derived within the optimization. Since the aim is to yield compact, yet performant EHA systems, the first assumption is that the hydraulic component radial dimension, including a bearing support, D_{brg}, matches the electric machine diameter D_s. With the same reasoning, the cylinder piston diameter D_p is relatable to the electric machine diameter. Exploiting data from a commercial bearing manufacturer [28] and considering an EHA application in automotive suspension systems, it is assumed that

$$D_{brg} = D_s,\ \ D_g = 0.65\ D_s,\ \ D_p = \ 0.3\ D_s \tag{6}$$

The first objective functions is the EHA volume, in favor of compactness and weight reduction. Only the electric and hydraulic machines volumes are considered as the hydraulic cylinder shape and size strongly depends on the application. The objective function is expressed as:

$$\begin{aligned} V_m = \frac{\pi}{4} D_s^2 L_m,\ V_g = \frac{\pi}{4} D_g^2 L_g - \ D_m, \\ F_1(\mathbf{X}) = V_{EHA} = V_m + V_g = \ f(D_s, L_g, L_m) \end{aligned} \tag{7}$$

where the electric machine volume V_m is calculated as if it was full of material, whereas the fluid volume D_m is subtracted to the gerotor volume.

The second objective function concerns the EHA efficiency. Namely, combining gerotor and electric machine efficiencies in nominal conditions, the formulation is as follows

$$F_2(\mathbf{X}) = -\eta_g \eta_m = f(D_s, L_g, L_m) \tag{8}$$

in which the minus sign is inserted so that the algorithm can perform an appropriate minimization.

Lastly, design constraints should be defined to bound the algorithm search space. First, the maximum angular speed of the electric machine is considered. Accounting for the cylinder specifications of Section 2.1 and the definition of transmission ratio τ, the constraint is formulated as

$$\begin{aligned} \tau = \frac{D_m}{Ap} = f(D_s, L_g), \\ g_1(\mathbf{X}) = \frac{v_{max}}{\tau} - \omega_{max} \le 0 \end{aligned} \tag{9}$$

in which the first term is derived from the cylinder linear velocity requirement; whereas, the second is its upper bound.

The second constraint is related to the gerotor volumetric displacement D_m. Recalling Eq.2 and the maximum power at the gerotor side P_{gmax}

$$\begin{aligned} P_{gmax} &= \frac{P_{max}}{\eta_c} = D_t\, \Delta p_{max}\, \omega_n, \\ D_t &= \frac{P_{max}}{\Delta p_{max}\, \omega_n} \\ g_2(\mathbf{X}) &= D_t - D_m \leq 0 \end{aligned} \tag{10}$$

in which ω_n represents the base speed, corresponding to the maximum torque condition for the electric machine and D_t is the target volumetric displacement. Eq.10 imposes a lower bound as the power requirement should be fulfilled.

The last constraint is presented in Eq. 11, bounding the torque transmission between electric and hydraulic sides. Namely, the objective is to constrain the transmission efficiency to be as high as possible.

$$\begin{aligned} g_3(\mathbf{X}) &= |w_1 T_m - w_2 T_g| \leq 0 \\ \text{where } w_1 &= \eta_m\ ,\ w_2 = \frac{1}{\eta_g} \end{aligned} \tag{11}$$

3. Optimization Results and Validation

The optimization framework presented in Section 2 is evaluated considering the design of an EHRSA for a car vehicle. The actuation requirements and the application assumptions are stated in Table 2, considering the reasonings of Section 2.

Concerning the genetic algorithm, the initial population size was set to 200 chromosomes, 80% of them is subject to crossover, the remaining to mutation. The maximum algorithm iterations are 100, whereas the tolerance in objective and constraints functions has been selected as 10^{-4} and 10^{-3}, respectively. Within the optimization framework, the geometrical constraints are

$$\begin{aligned} 30 \ &\leq\ D_s \ \leq\ 150\ [\text{mm}] \\ 5 \ &\leq\ L_g \ \leq\ 100\ [\text{mm}] \\ 20 \ &\leq\ L_m \ \leq\ 100\ [\text{mm}] \end{aligned} \tag{12}$$

Table 2: EHA prototype case study

Symbol	Value	Description
F_{max}	2000 N	Maximum actuator force
F_{min}	100 N	Minimum actuator force
v_{max}	0.8 m/s	Maximum actuator speed
v_{min}	0.1 m/s	Minimum actuator speed
P_{max}	500 W	Maximum actuator power
D_g	$0.65D_s$	Gerotor diameter
D_p	$0.3D_s$	Linear actuator piston diameter
ω_{max}	20 krpm	PMSM maximum angular speed
ω_n	10 krpm	PMSM nominal angular speed
η_{em}	0.9	PMSM efficiency at maximum torque

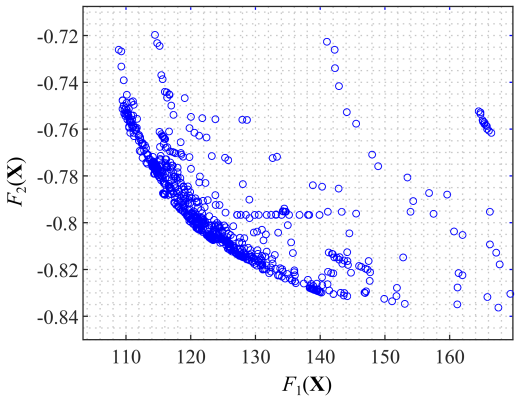

Figure 4: Solutions space in the objective functions plane

Fig. 4 presents the optimization outcome in the objective functions plane. $F_1(\mathbf{X})$ represents the EHA volume [cm^3], whereas $F_2(\mathbf{X})$ is the overall EHA efficiency with the minus sign. The two are inversely proportional, as expected. Therefore, the algorithm aims at finding an optimal trade-off among the two, based on the constraints imposed. Fig. 5 presents the Pareto front of the algorithm versus the design variables. Black dots refer to the entire three-dimensional Pareto front. The x axis concerns the electric machine diameter D_s, gerotor length L_g in y direction and electric machine active length L_m representing the z axis. In the x-z plane, the projection of the optimal solutions is presented with blue dots. L_m and D_s are inversely proportional. Such behavior can be justified considering that the volume objective function quadratically depends on the diameter and linearly on the axial length. Therefore, the algorithm tries to first minimize the diameter to reduce the EHA volume. On the other hand, the efficiency objective favors the increase in axial length over that in electric machine diameter. Then, the x-y plane (i.e., red dots) relates the Pareto front to electric machine diameter D_s and gerotor length L_g. The latter approaches a lower bound, constraining the search space of the algorithm. Conversely, the y-z plane (i.e., green dots) relates the Pareto front to gerotor length L_g and electric machine active length L_m. A variation in terms of L_m does not cause substantial change in gerotor length L_g, approaching its geometrical lower bound. Additionally, data points highlighting a direct proportionality between L_m and L_g are present.

Finally, Fig. 5 remarks with a yellow circle the location of

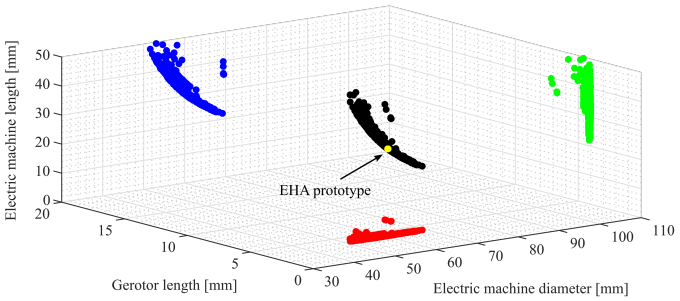

Figure 5: Pareto front of the MOO problem

Table 3: EHA prototype design parameters

Symbol	Value	Description
D_s	70 mm	Electric machine diameter
L_m	22 mm	Electric machine length
D_g	45 mm	Gerotor diameter
L_g	6 mm	Gerotor axial length
D_m	2.5 cm^3/rev	Gerotor volumetric displacement
D_p	22 mm	Linear cylinder piston diameter

the optimal solution chosen to design the EHA prototype and Table 3 presents the optimization parameters.

3.1. Numerical Validation

The gerotor component is investigated by means of CFD analyses, simulating the fluid volume behavior in two different configurations: working as motor and as pump. Pumping operations are characterized by the electric machine imposing torque and the gerotor pressure differential resisting such load, II and IV quadrants of the force-speed plane; whereas, if the gerotor pressure differential is generating torque and the electric machine is resisting the load (usual scenario in suspension systems), the gerotor behaves as an hydraulic motor, exploring I and III quadrants.

The CFD analysis is set up considering positive force and varying the gerotor angular speed from negative to positive values as the gerotor energetic behavior can be considered symmetrical with respect to force. Simerics PumpLinx is exploited as simulation environment, considering a fluid density ρ of 840 [kg/m^3] and a dynamic viscosity μ_f of 9400 [Pa/s], common characteristics of fluids used in hydraulic suspension systems. The maximum number of iterations per each simulation is set to 100, whereas the time steps per each fluid chamber is fixed to 20. Ten, equally spaced angular speed ω_g values between -20 krpm to 20 krpm are evaluated; whereas five pressure differentials Δp, from 5 to 50 bar are imposed between gerotor inlet and outlet ports. For each simulation, the 3D fluid model is solved for an angular motion transient equal to four hydraulic chambers, to avoid effects related to transient conditions. Both radial and axial clearances were accounted in the simulation. Radially, the clearance was set to $c_{rad} = 10$ μm to account for viscous losses between gerotor and its envelope; whereas, the axial one was set to $c_{ax} = 20$ μm for each side, assuming uniform gap distribution. No axis misalignment or gears deformation effects were considered. To connect meshed volumes, mismatched grid interfaces were implemented. In each simulated point, the efficiency is calculated according to

$$\eta_{gm} = \frac{T_g\,\omega_g}{\Delta p\,Q_g}, \qquad \eta_{gp} = \frac{\Delta p\,Q_g}{T_g\,\omega_g} \tag{13}$$

in which η_{gm} is for gerotor motoring operations (i.e., I quadrant) whereas η_{gp} for pump behavior (i.e., II quadrant). The analysis outcomes are torque and flow rate, extrapolated considering a gridded interpolation. Efficiency results were post-processed

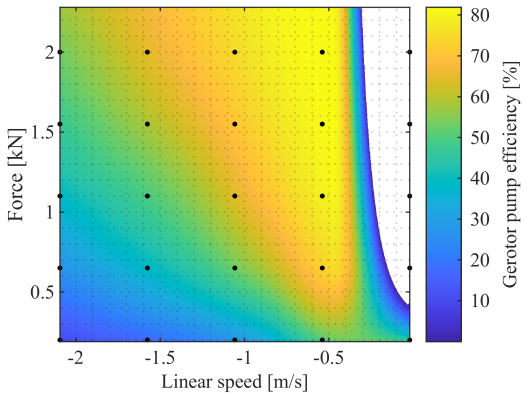

(a) Pump

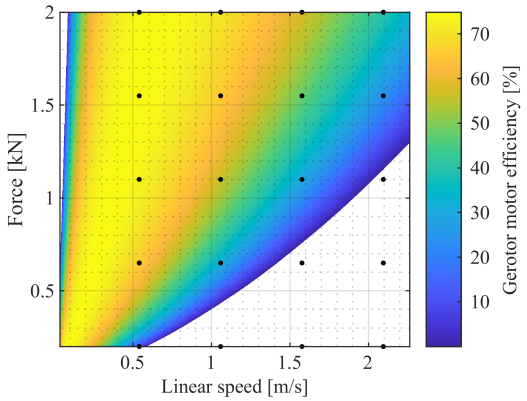

(b) Motor

Figure 6: Gerotor unit efficiency maps. Black dots represent simulated points whereas the colormap is the result of a gridded interpolation.

with a piece-wise cubic interpolation function and presented in Fig. 6.

Overall, the maximum efficiency is approximately 75% in both operating conditions. Hydraulic and mechanical losses are present in both conditions. The latter are represented by an inclination of the map with respect to the vertical axis. Namely, at low speeds and high forces the gerotor is not able to win friction losses, resorting in null efficiency. Conversely, the effect of hydraulic losses is an inclination of the map with respect to the speed axis. No efficiency characterizes low force and high speed operating points as hydraulic leakages dominate the gerotor fluid dynamic behavior. Moreover, the sealing capabilities of the gerotor working as pump are better than those in motoring operations. Additionally, the efficiency in both conditions is affected by the clearances definition. Tighter gaps favor volumetric over mechanical efficiency; whereas, larger gaps decrease viscous drag at the cost of increased hydraulic leakages.

On the other hand, FEM models are exploited to preliminary evaluate the electric machine efficiency working as motor and generator. Fig. 7 presents the PMSM efficiency maps, extrapolated by means of a shape preserving piece-wise cubic function. In both working conditions, the maximum efficiency is around 90%, corresponding to the machine nominal operating condition. Similarly to the gerotor, the electric machine is

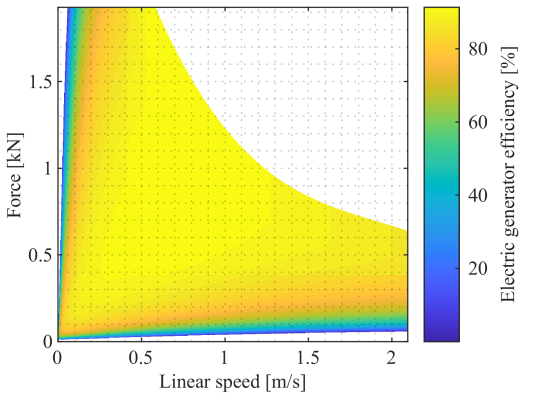

(a) Generator

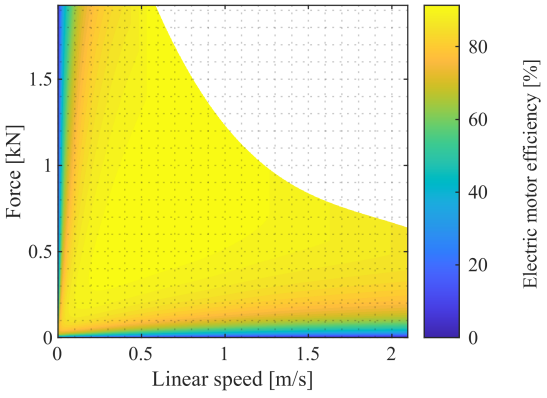

(b) Motor

Figure 7: Electric machine efficiency maps

not able to efficiently operate in every working condition, as specific operating points (i.e., low speed - high force and high speed - low force pairs) are inefficient. In both conditions, the generated electric power is lower than core and Joule losses.

3.2. Experimental Validation

Fig. 8 shows the testbench setup used to evaluate the fully custom EHRSA design. A motor-pump unit drives the hydraulic circuit while the EHRSA resists the load, reproducing different damping responses. A FOX GR2 gas-loaded accumulator is used to stabilize the pressure in the hydraulic circuit, preloaded to avoid cavitation problems. Tests were performed in the I quadrant of the Force-speed plane; thus, the gerotor is working as motor while the electric machine as generator. The driving unit features a Kollmorgen AKM42G brushless PM motor coupled to a Casappa PLP10 pump. The prototype is controlled by means of a dedicated power stage, connected to four lithium-ion batteries (12 V) in series. The battery is both used to power the prototype's electronics as well as to harvest energy generated by the electric machine. Moreover, the test rig includes two pressure sensors (GEFRAN TK) to measure the pressure differential across the prototype and a turbine flow meter (HYDAC EVS 3100). Voltage is measured through the battery management system, whereas a dedicated probe measures phase current. Then, Hall sensors are used to measure the angular speed of the electric machine as well as to implement a field-oriented control (FOC) strategy. Lastly, LMS SCADAS is used to acquire data. The procedure to conduct the test is as follows:

1. The driving motor-pump unit is controlled to work at constant angular speed;
2. The power stage imposes a set of reference current values to the prototype, that can be translated to a set of constant damping forces for the actuation system;
3. For each current value, sensor measurements are acquired;
4. The driving motor angular speed is varied and the acquisition procedure is repeated (Steps 1-3);
5. Sensors data are interpolated and used to extrapolate the EHA efficiency maps.

Tests were performed exploring a range of motor-pump driver angular speeds between 3 to 6 krpm. The lower bound is dictated by the turbine flow meter. Its lowest, significative measure Q_{minf} is 6 l/min. Hence, the least explorable angular speed of the EHA prototype is

$$Q_{minf} = D_m\, \omega_{min},\ \omega_{\min} = 2500 \text{ rpm} \tag{14}$$

On the other hand, the driving motor nominal working conditions limits the maximum explorable angular speed. In fact, by comparing the volumetric displacements of driving pump, $D_{md} = 2.15$ cm^3/rev, and gerotor machine, $D_m = 2.5$ cm^3/rev,

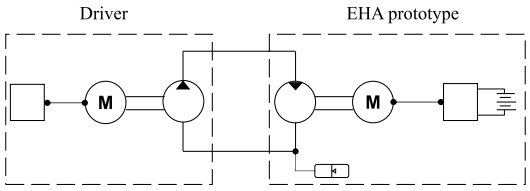

(a) Test rig scheme

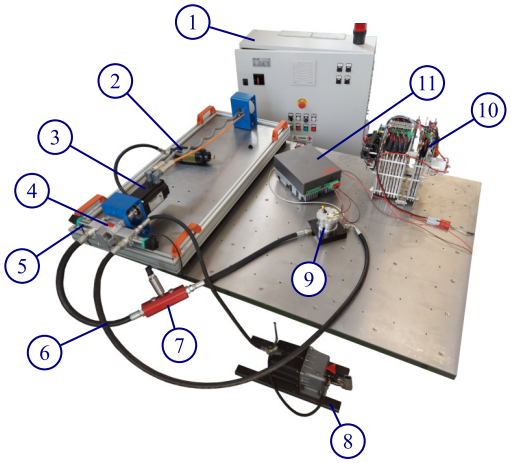

(b) Test rig setup

Figure 8: Test rig. Inverter (1), Gas-loaded accumulator (2), Driving motor (3), Driving pump (4), Pressure sensors (5), Hydraulic lines (6), Flow meter (7), Preload hand pump (8), EHA prototype (9), Battery stage (10), Power electronics (11).

it is possible to compute the maximum testable EHA angular speed

$$
\begin{aligned}
Q_{maxd} &= D_{md}\ \omega_n, \\
Q_{max} &= \eta_p\ D_m\ \omega_{max}, \\
\omega_{max} &= \frac{D_{md}}{\eta_p\ D_m}\ \omega_n = 5500 \text{ rpm}
\end{aligned}
\tag{15}
$$

in which Q_{maxd} is the driving pump maximum flow rate and η_p is the hydraulic lines efficiency (assumed to be 95%). Lastly,

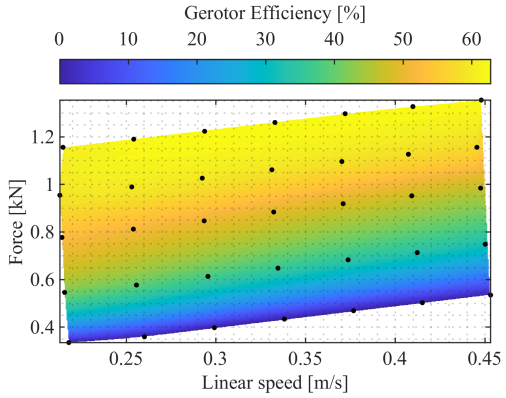

(a) Gerotor unit

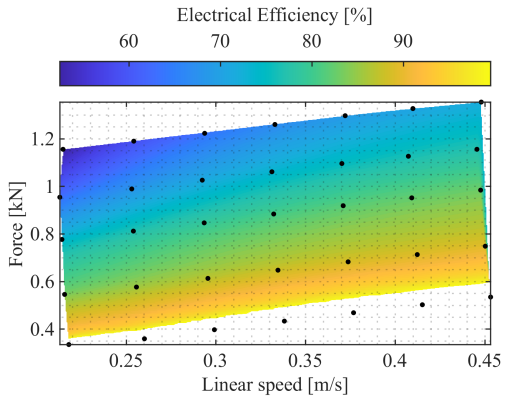

(b) Electric machine

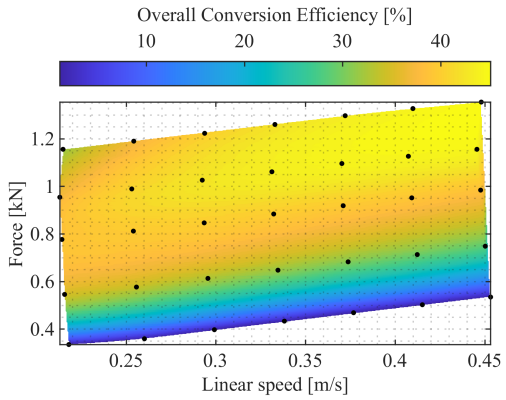

(c) Overall

Figure 9: Experimental prototype efficiency maps

Table 4: Quarter car model parameters

Symbol	Value	Description
m_s	416.5 kg	Sprung mass
m_u	40 kg	Unsprung mass
k_s	23.256 kN/m	Sprung mass stiffness
k_u	226 kN/m	Unsprung mass stiffness

from a damping perspective, current values ranging between 0 to 20 A were tested to provide cylinder forces between 0 and 1500 N.

Fig. 9 presents the efficiency experimental maps considering gerotor, electric machine and overall actuation unit. The gerotor efficiency tends to be null at low force content. Since the damping content is low while the angular speed is increasing, hydraulic leakages dominate the efficiency map. Conversely, the efficiency reaches its maximum, (i.e., 65 %) for high damping forces. On the other hand, the electrical efficiency map has an opposite behavior. As the damping content increases, the electric machine works closer to the short-circuit damping condition; thus, electrical losses due to Joule effect severely affect the efficiency. Instead, as the damping content is close to zero, the power stage imposes less current, the impedance increases and the efficiency tends to the unit. Finally, the overall conversion efficiency is the product of the previous two. The maximum value is around 45%, in line with EHRSA systems used in high duty cycle operations. Hydraulic losses are predominant at low damping force; whereas, the electric machine working close to the short-circuit condition affects the overall efficiency at high damping content.

3.3. EHRSA Energy harvesting analysis

The energy harvesting capabilities of the prototype have been tested considering a quarter car model. The objectives were to: (i) guarantee proper suspension handling and comfort performance and (ii) maximise energy regeneration. The quarter car model main parameters are summarized in Table 4, representing a J-class vehicle. Figure 10 provides a schematic of the closed-loop control strategy implemented. The road profile and damping force are the model inputs, whereas suspension position x, velocity $\dot{x}$ and acceleration $\ddot{x}$ of sprung and unsprung masses are the outputs. The latter are fed to the control strategy to generate the reference force and speed for the EHA. The con-

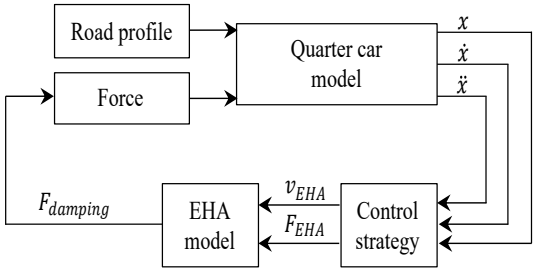

Figure 10: Quarter car control loop

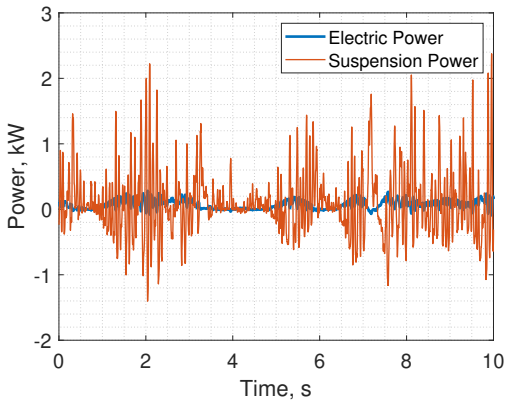

Figure 11: Power comparison: suspension power (red), electric power (blue).

trol loop is closed generating the required suspension damping force.

A band-limited white noise, filtered considering road condition (class C) and vehicle longitudinal speed (70 km/h) is exploited to model the road profile. Then, the experimental efficiency maps extrapolated from Figure 9 are exploited to model the regenerative shock absorber behaviour. Reflected inertia and dry friction contributions have been included in the model. Finally, a linear quadratic regulator (LQR) control has been empirically tuned to maximize the energy regeneration of the suspension system.

Figure 11 presents the comparison between suspension and PMSM electric powers for a 10 seconds time window. Regenerated power is positive whereas EHRSA actuation is represented by the negative sign. Quantitatively, the regeneration efficiency is around 20.5%, in line with state of the art regenerative shock absorbers tested in real case scenarios [2]. Moreover, it is possible to estimate a reduction in vehicle CO_2 emissions based on regenerated power. According to the European technical guidelines for eco-innovation [29], an estimate of the emission savings is

$$S_{CO_2} = \frac{n_{sa} P_g V_{Pe} C_f}{\eta_a v_{car}} \tag{16}$$

in which $n_{sa} = 4$ is the number of shock absorbers, P_g is the average regenerated power (101 W), $V_{pe} = 0.22$ l/kWh is the fuel consumption of effective power for diesel, $C_f = 2640$ g/l is a factor that considers the fuel convertion into CO_2, $\eta_a = 0.67$ is the alternator efficiency and $v_{car} = 70$ km/h is the vehicle longitudinal speed. Considering Eq. 16, the CO_2 estimate is around 5 g/km of savings, representing 5.25% of the 2020 CO_2 emission bound.

4. Conclusion

The conducted research presented an optimized framework for the design of electro-hydrostatic regenerative shock absorbers. By mathematically modeling a multi-objective optimization problem, an evolutionary genetic algorithm was implemented to find a set of optimal design solutions. The methodology has been validated in two different ways. Numerically, fluid dynamic simulations of the gerotor presented the efficacy of the optimized methodology, leading to a performant and compact gerotor unit (i.e., 75% maximum efficiency). On the other hand, electromagnetic finite element simulations validated the electric machine design, working both as motor and generator (90% maximum efficiency). Then, a prototype was manufactured and experimentally tested. Experimental results showed the ability of the prototype to deal with working conditions pertaining to a suspension system with adequate performance and contained size (45% maximum conversion efficiency).

Finally, the energy regeneration performance has been validated considering a quarter car model and a control strategy that guarantees appropriate vehicle handling and comfort. A 5g/km estimate of CO_2 reduction was found, representing 5.25% of the 2020 CO_2 vehicle emission bound.

Therefore, the optimization methodology presented within this study is able to yield a compact and performant active, regenerative shock absorber with elevated power harvesting and regeneration capabilities.

Future works will aim at integrating the developed prototype on an actual suspension system and perform experimental testing on an instrumented vehicle to further evaluate the energy regeneration capabilities.

References

[1] EU, Regulation (eu) 2019/631 of the european parliament and of the council of 17 april 2019 setting co2 emission performance standards for new passenger cars and for new light commercial vehicles, and repealing regulations (ec) no 443/2009 and (eu) no 510/2011 (2019).
URL http://data.europa.eu/eli/reg/2019/631/oj

[2] M. Abdelkareem, L. Xu, M. Ali, A. Elagouz, J. Mi, S. Guo, Y. Liu, L. Zuo, Vibration energy harvesting in automotive suspension system: A detailed review, Journal of Applied Energy 229 (2018). doi:https://doi.org/10.1016/j.apenergy.2018.08.030.

[3] ISO8608, Mechanical vibration — road surface profiles — reporting of measured data (2016).
URL https://www.iso.org/standard/71202.html

[4] Z. Lei, Z. P. Shang, Energy harvesting, ride comfort, and road handling of regenerative vehicle suspensions, Journal of Vibrations and Acoustics 135 (2013). doi:https://doi.org/10.1115/1.4007562.

[5] R. Galluzzi, A. Tonoli, N. Amati, et al., Regenerative shock absorbers and the role of the motion rectifier, SAE technical paper (2016). doi:https://doi.org/10.4271/2016-01-1552.

[6] R. Hanitsch, Rotary and linear machines, Encyclopedia of Materials: Science and Technology (2001) 8221–8227doi:https://doi.org/10.1016/B0-08-043152-6/01472-8.

[7] A. Tonoli, N. Amati, J. Girardello Detoni, R. Galluzzi, E. Gasparin, Modelling and validation of electromechanical shock absorbers, Vehicle System Dynamics 51 (8) (2013) 1186–1199. doi:https://doi.org/10.1080/00423114.2013.789538.

[8] R. Galluzzi, S. Circosta, N. Amati, A. Tonoli, Rotary regenerative shock absorbers for automotive suspensions, Mechatronics 77 (2021). doi:https://doi.org/10.1016/j.mechatronics.2021.102580.
URL https://www.sciencedirect.com/science/article/pii/S0957415821000672

[9] Z. Zutao, Z. Xingtian, C. Weiwu, R. Yagubov, S. Waleed, H. Pan, Y. Yanping, W. Chunbai, A high-efficiency energy regenerative shock absorber using supercapacitors for renewable energy applications in range extended electric vehicle, Applied Energy 178 (2016) 177–188. doi:https://doi.org/10.1016/j.apenergy.2016.06.054.

[10] D. Belloli, F. Previdi, S. Savaresi, A. Cologni, M. Zappella, Modeling and identification of an electro-hydrostatic actuator, IFAC Proceedings Vol-

umes 43 (18) (2010) 620–625. doi:10.3182/20100913-3-US-2015.00020.

[11] N. Alle, S. Hiremath, S. Makaram, K. Subramaniam, A. Talukdar, Review on electro hydrostatic actuator for flight control, International Journal of Fluid Power 17 (2) (2016) 125–145. doi:10.1080/14399776.2016.1169743.

[12] R. Galluzzi, N. Amati, A. Tonoli, Modeling, control, and validation of electrohydrostatic shock absorbers, Journal of Vibrations and Acoustics 137 (2015). doi:https://doi.org/10.1115/1.4028310.

[13] Z. Yuxin, C. Hong, G. Konghui, Z. Xinjie, E. L. Shengbo, Electro-hydraulic damper for energy harvesting suspension: Modeling, prototyping and experimental validation, Applied Energy 199 (2017) 1–12. doi:10.1016/j.apenergy.2017.04.085.

[14] H. Kaminaga, A. Tomoya, Y. Niwa, N. Yoshihiko, Electro-hydrostatic actuators with series dissipative property and their application to power assist devices, 3rd IEEE RAS & EMBS International Conference on Biomedical Robotics and Biomechatronics (2010) 76–81.

[15] F. Tessari, R. Galluzzi, A. Tonoli, N. Amati, G. Milandri, M. Laffranchi, L. De Michieli, An integrated, back-drivable electro-hydrostatic actuator for a knee prosthesis, 2020 8th IEEE RAS/EMBS International Conference for Biomedical Robotics and Biomechatronics (BioRob) (2020) 708–714doi:10.1109/BioRob49111.2020.9224278.

[16] M. Puliti, F. Tessari, R. Galluzzi, et al., A hybrid swing-assistive electro-hydrostatic bionic knee design, 9th IEEE RAS/EMBS International Conference for Biomedical Robotics and Biomechatronics (BioRob), Seoul, Republic of Korea (2022) 01–07doi:10.1109/BioRob52689.2022.9925422.

[17] S. Alfayad, F. Ouezdou, F. Namoun, G. Gheng, High performance integrated electro-hydraulic actuator for robotics – part i: Principle, prototype design and first experiments, Sensors and Actuators A: Physical 169 (1) (2011) 115–123. doi:10.1016/j.sna.2010.10.026.

[18] R. Navarro, Performance of an electro-hydrostatic actuator on the f-18 systems research aircraft, Report No. NASA/TM-97-206224 (1997).

[19] F. Tessari, R. Galluzzi, N. Amati, Efficiency-driven design methodology of gerotor hydraulic units, ASME Journal of Mechanical Design 142 (6) (2019) 063501. doi:10.1115/1.4045421.

[20] R. Galluzzi, Y. Xu, N. Amati, A. Tonoli, Optimized design and characterization of motor-pump unit for energy-regenerative shock absorbers, Applied Energy 210 (2018) 16–27. doi:10.1016/j.apenergy.2017.10.100.

[21] H. Yanada, T. Uchino, T. Takeno, R. Kojima, H. Yokoyama, Rotor Behavior and Friction Torque Characteristics of a Gerotor Pump Used for Automatic Transmissions, Journal of Dynamic Systems, Measurement, and Control (07 2021). doi:10.1115/1.4051644.

[22] M. Rundo, Models for flow rate simulation in gear pumps: A review, Energies 10 (2017) 1261. doi:10.3390/en10091261.

[23] P. Gamez-Montero, R. Castilla, E. Codina, Methodology based on best practice rules to design a new-born trochoidal gear pump, Proceedings of the Institution of Mechanical Engineers, Part C: Journal of Mechanical Engineering Science 232 (6) (2018) 1057–1068. doi:10.1177/0954406217697355.

[24] M. Puliti, F. Tessari, R. Galluzzi, A. Tonoli, N. Amati, Design methodology of gerotor hydraulic machines for mechatronic applications, ASME International Mechanical Engineering Congress and Exposition (2021). doi:https://doi.org/10.1115/IMECE2021-73205.

[25] J. Harrison, R. Aihara, F. Eisele, Modeling gerotor oil pumps in 1d to predict performance with known operating clearances, SAE International Journal of Engines 9 (3) (2016) 1839–1846. doi:10.4271/2016-01-1081.

[26] D. C. Hanselman, Brushless Permanent Magnet Motor Design, Magna Physics Publishing, 2006.

[27] G. Liu, X. Han, C. Jiang, A novel multi-objective optimization method based on an approximation model management technique, Computer Methods in Applied Mechanics and Engineering 197 (33) (2008) 2719–2731. doi:10.1016/j.cma.2007.12.014.

[28] SKF, Rolling bearings (2021).
URL https://www.skf.com/us/products/rolling-bearings

[29] European, Commission, Technical guidelines for the preparation of applications for the approval of innovative technologies pursuant to regulation (ec) no 443/2009 of the european parliament and of the council (Rev. 2013).